Desalination and Water Treatment
www.deswater.com
doi: 10.5004/dwt.2020.24850

174 (2020) 11–25
January

Performance evaluation and economic assessment of a gas power plant with solar and desalination integrated systems

S. Hoseinzadeh[a,c,*], R. Ghasemiasl[b], M.A. Javadi[a], P.S. Heyns[c]

[a]*Young Researchers and Elite Club, West Tehran Branch, Islamic Azad University, Tehran, Iran, emails: hoseinzadeh.siamak@gmail.com/Hosseinzadeh.siamak@up.ac.za (S. Hoseinzadeh)*
[b]*Department of Mechanical Engineering, West Tehran Branch, Islamic Azad University, Tehran, Iran*
[c]*Centre for Asset Integrity Management, Department of Mechanical and Aeronautical Engineering, University of Pretoria, Pretoria, South Africa*

Received 24 November 2018; Accepted 1 September 2019

ABSTRACT

In this study, a new configuration of a cogeneration system of electricity and freshwater in integration with solar collector has been thoroughly investigated. A gas power plant is modeled thermodynamically. The results of this modeling are compared with the actual data of a power plant to verify the simulation. Subsequently, by placing multi-effect desalination with thermal vapor compression and solar collectors, the functions including energy and exergy efficiencies and carbon dioxide emissions of the power plant have been studied. By applying the desalinating cycle and solar collectors, the energy efficiency of this power plant is increased from 35% to 46% and the exergy efficiency from 37% to 48%. This configuration of the cogeneration system with linear solar collectors produces 16.479 m^3 of fresh water per day while reducing the CO_2 emissions by 37,216 tons/d.

Keywords: Thermal desalination; Exergy; Energy; Gas turbine; Cogeneration system; Linear solar collector

1. Introduction

In 2016 Bellos et al. [1] investigated the properties of active fluids in parabolic solar collectors. Based on a predesignated model, properties such as density, specific heat, viscosity, thermal conductivity, and heat transfer coefficient for different active fluids at different temperatures were obtained. Thermal analysis was carried out using engineering equation solver tools. In this article, the performance of the parabolic solar collector was investigated using the Eurotrough ET-150 model for seven different active fluids, namely pressurized water, Therminol VP-1, nitrate molten salt, sodium liquid, air, carbon dioxide, and helium. Their experiments showed that the parabolic solar collector can work with all these active fluids. This research has been conducted at high temperatures from 300 to 1,300 K, and each active fluid has been tested in the feasible range of temperatures. Additionally, for each active fluid, a sensitivity analysis was performed and the flow rate was set to achieve the best performance. The final results indicate that liquid active fluids perform better than the gas active fluids, and at a low temperature around 550 K high-pressure water is the most viable choice. Another finding was that sodium liquid is suitable for high temperatures up to 1,100 K. Finally, carbon dioxide and helium were shown to be most suitable for temperatures above 1,100 K.

Sanaye et al. [2] published research on the modeling and optimization of combined cycle gas turbines with steam spraying in the combustion chamber. In this work, the gas turbine cycle was modeled, including sections of the compressor, turbine, combustion chamber, and heat recovery boiler, in order to obtain the optimal design parameters for generating the required power, assuming an objective function of initial investment and fuel costs. The design parameters include the turbine input temperature, the compressor compression ratio, the isentropic compressor and turbine

* Corresponding author.

efficiency, the pinch temperature difference in recovery, and the mass flow rates of vapor and air.

Kahraman and Cengel [3] performed an exergy analysis on multi-effect flash distillation. In this analysis, it is shown that the highest calculated destruction of exergy at 77.7% can be reduced by increasing the number of steps. The exergy destruction of pumps and motors was calculated at about 5.3%, which can be reduced by increasing the efficiency of motors and pumps. Therefore, the supplied electricity and thermal energy will make the device more efficient.

Shakib et al. [4] simulated and optimized a multi-effect desalination unit that was coupled with a gas turbine cycle and furnished with a recovery boiler. In 4, 6, and 8-effect desalination units increasing the water temperature from 20°C to 50°C increase the production rate of fresh water by about 4%, 5%, and 6% respectively. Increasing the water intake temperature at the recovery boiler decreases its exergy destruction. However, this increases exergy destruction in the desalination unit. Also, increasing the number of desalination steps for a given temperature reduces exergy destruction. By increasing the steam pressure from 300 to 4,200 kPa, the exergy destruction decreases in the recovery boiler and increases in the desalination process. The efficiency of desalination reaches its maximum at a specific pressure. For desalination units with 4, 6, and 8 steps, this is attained at about 1,500 kPa. At lower and higher pressures, the efficiency drops.

Maghsoudi et al. [5] in 2016 studied the exergy optimization in the Shahid Rajaee Steam-Electric Power Plant with a feedwater heater, using a genetic algorithm. The sensitivity of the objective function with respect to variations of the output rates for existing steam turbines was analyzed using a genetic algorithm to determine the optimal output rate. The overall exergy efficiency was determined by calculating exergy loss and efficiency for each part [6]. It was determined that increasing the turbine load by 25 MW improves energy and exergy efficiencies by up to 5% and results in an overall efficiency increase for the entire power generation cycle of 7%.

The properties of sodium liquid were obtained from an article by Fink et al. [7] on the calculation of sodium liquid properties. The models for sodium liquid and hot air heat exchangers come from a research article by Ariu [8].

Sharif [9] examine the efficiency and cost of electricity generated by conventional combined cycle power plants. In the second part, the hybrid system of the gas turbine power station and renewable energies, such as onshore and offshore wind turbines and photovoltaic solar cells, are investigated. In the third part, they also examine alkaline electrolytes. The research shows that the conventional combined cycle power plant is less expensive, however, the alternative, namely the hybrid system, has higher efficiency and lower emissions of greenhouse gases.

Al-Mutaz and Wazeer [10] focus on the mathematical modeling of multi-effect desalination with thermal vapor compression (MED-TVC) desalinators. Balance equations of mass, energy and heat transfer related to different components were implemented in MATLAB and results were obtained.

For this research, the basic principles of thermodynamics and desalination have been considered with various journal articles on parabolic solar collectors, combined gas and solar power plants [11–14], high-temperature heat exchangers, sodium liquid properties, combining power plants and desalination units. Resulting from these studies, a design was conceived in which a parabolic solar collector is placed between the compressor and the combustion chamber to preheat the compressor's outlet air to increase the temperature in the combustion chamber. The compressor inlet air temperature and pressure as well as its compression ratio were assumed to be known. Consequently, the compressor's outlet temperature, the heat transfer at the parabolic collector, and the air temperature increase at compressor outlet are determined based on thermodynamic identities [15–17]. The solar collector is a linear parabolic system with sodium liquid as the active fluid which circulates within the focal tube and collects the heat that will later be transferred to the air in heat exchangers. The compressor outlet air is preheated before entering the combustion chamber, and the dissipated hot gas from the turbine will be used for water desalination. To accomplish the above-mentioned steps, each part of the cycle was modeled and then implemented in MATLAB and the results are obtained and illustrated [18–20].

Using computational methods in thermodynamic and exergy analysis for a combined system of power generation and desalination, the influence of operational parameters of the recovery boiler on the desalination unit was investigated. Deriving the governing equations on different sections, various results were presented as diagrams and in different forms and the following general results were obtained. Higher salt concentrations and temperatures increase the exergy of in desalination unit. This increases at higher temperatures. However, the performance of the system, although similar to the exergy efficiency, improves at increasing brine temperature, but decreases with increasing salt concentrations. The highest percentage of exergy destruction in the desalination process is related to the steam ejectors and in the power generation cycle at the combustion chamber and, after that, at the turbine and the compressor.

2. Desalination plant modeling

The proposed model is a multi-effect parallel feed thermal vapor compression desalination system consisting of many evaporators, a steam jet ejector, flashing boxes, and an end condenser (to condensate the steam produced in the last effect [21]). The schematics of this model is illustrated in Fig. 1.

The role of the end condenser is the disposal of excess heat from the system. After the water is fed into the system with flow rate of $m_{cw} + m_f$ and temperature T_{cw}, the temperature of the water increases to T_f due to heat exchange from the steam in the pipes, and a portion of it is disposed from the system as cooling water, while the remainder enters the evaporator with flow rate of m_f. Some of the water is evaporated due to the heat of the steam in the pipes. The produced steam enters and flows in its evaporator effect. This process is repeated for each of the n effects. The following assumptions are used for the desalination system:

- Steady-state operation of the system
- Physical properties of all the flows are calculated using the temperature of each input and output

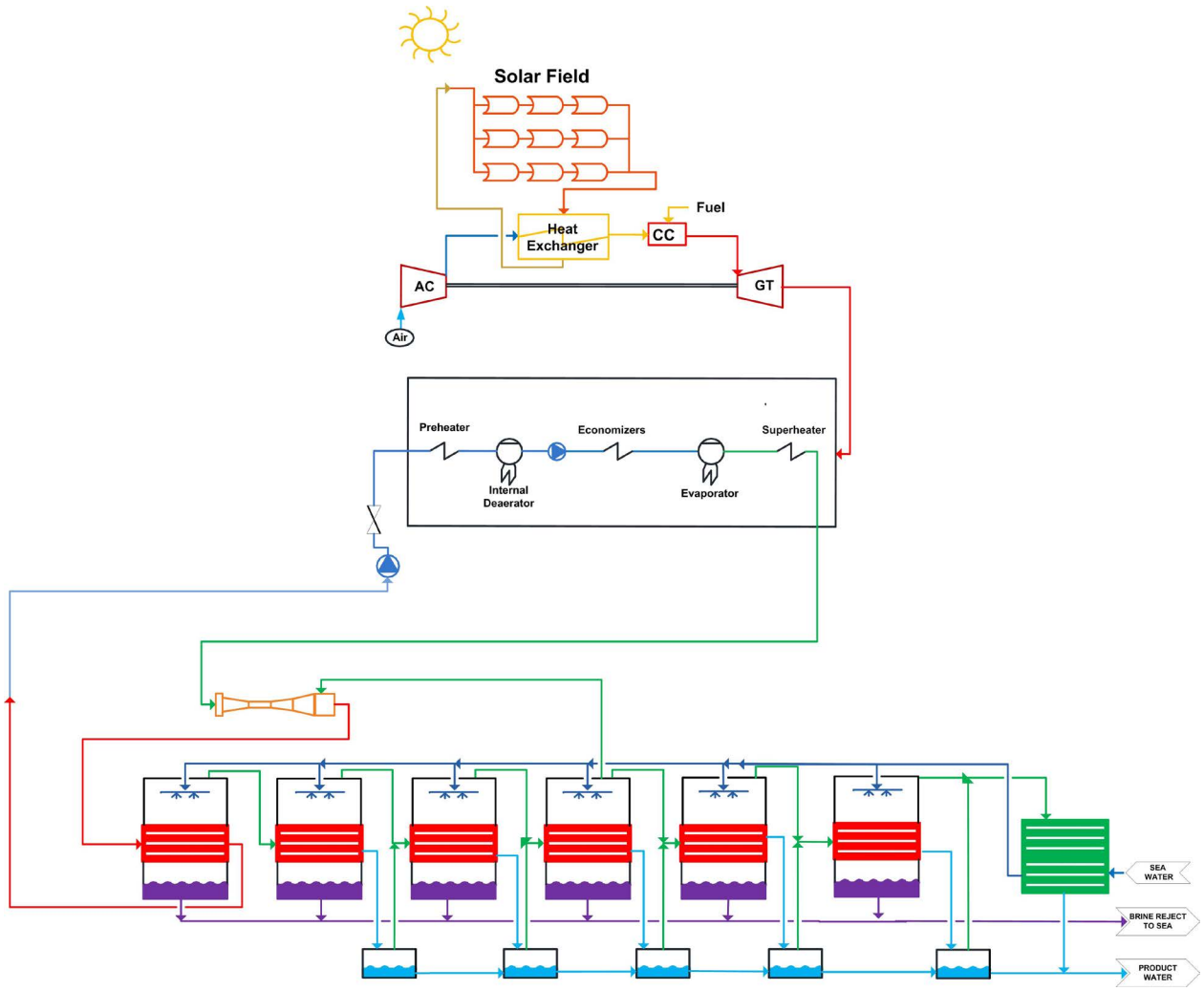

Fig. 1. Multi-effect evaporation with thermal vapor compression desalination system (MEE-TVC).

- Steam produced in each effect is salt-free
- Heat exchange with the environment is negligible
- Boiling point elevation (BPE) is equal for all effects
- Dissolved salt percentage of the final wastewater is less than 70,000 ppm for environmental considerations
- Dissolved salt percentage of the wastewater of each state is so that the sedimentation is minimum
- Heat exchange areas of evaporators 2 to n are equal

The flow rate of the brine entering each of the effects is constant and is defined as:

$$F = \frac{M_f}{N} \tag{1}$$

The temperature difference between two consecutive effects is constant, and assuming the motive steam temperature to be T_s and the temperature of the last effect to be T_N, we get:

$$\Delta T = \frac{T_s - T_N}{N} \tag{2}$$

$$T_1 = T_s - \Delta T \tag{3}$$

$$T_{i+1} = T_i - \Delta T \tag{4}$$

$$i = 2 \ldots N \tag{5}$$

The mass balance in all the effects of the system is:

$$M_f = M_b + M_d \tag{6}$$

$$X_f M_f = X_b M_b \tag{7}$$

and the steam heating of the first effect of the desalination system supplied from the power station cycle is equal to the heat value Q. Therefore, the equation of energy balance is as follows:

$$Q = m_S\left(h_{s_{\text{out}}} - h_{s_{\text{in}}}\right) = m_f C_p (T_i - T_f) + m_{d_1}\lambda_{v_1} \tag{8}$$

$$m_{d_{i-1}}\lambda_{v_{i-1}} = m_f C_p (T_i - T_f) + m_{d_i}\lambda_{v_i} \quad (9)$$

In the above relations, X is the percentage salinity, h is the enthalpy in kJ/kg K, and the subscripts f, b, d, and s are related to the water supply, the saltwater discharged from each effect, and the steam formed at each effect. The value of λ_{vi} is the latent heat of evaporation at temperature T_{vi}. The steam temperature at each effect is lower than the boiling point by the BPE. The BPE value can be calculated as follows:

$$\text{BPE} = AX + BX^2 + CX^3 \quad (10)$$

$$A = (8.325 \times 10^{-2} + 1.883 \times 10^{-4}T + 4.02 \times 10^{-6}T^2) \quad (11)$$

$$B = (-7.625 \times 10^{-4} + 9.02 \times 10^{-5}T - 5.2 \times 10^{-7}T^2) \quad (12)$$

$$C = (1.522 \times 10^{-4} - 3 \times 10^{-6}T - 3 \times 10^{-8}T^2) \quad (13)$$

It is also possible to obtain the following relationships by using the definition of the total heat transfer coefficient of the evaporator and the condenser.

LMTD is the logarithmic mean temperature difference for the condenser. The total heat transfer coefficient of the evaporators and terminal condensers is equal to (subscripts e and c refer to the evaporator and end condenser):

$$Q_e = U_e A_e \Delta T_i \quad (14)$$

$$Q_c = U_c A_c \text{LMTD}_c \quad (15)$$

Fig. 2 shows a schematic image of the system variables in the evaporator and the flash box for step i. The shape contains flow rates, salinity, and different flow temperatures, during evacuation and exit from the flash box. Also, Fig. 3 shows a schematic of gas turbine cycle with solar collector.

3. Equations of equilibrium for each effect

The balance of salt and water in step i is

$$F_i + B_{i-1} = D_i + B_i \quad (16)$$

$$X_{F_i}F_i + X_{B_{i-1}}B_{i-1} = X_{B_i}B_i \quad (17)$$

In Eqs. (16) and (17) B, D, and F are salty water, freshwater, and water supply. X is the percentage salinity and subscripts B, F, and i denote saltwater, water supply, and the step number.

The percentage of brine washed out

$$X_b = 0.9(457628.5 - 11304.11T_b + 107.5781T_b^2 - 0.360747T_b^3) \quad (18)$$

This equation is used to calculate the salinity of the water discharged from each step as a function of brine temperature and is used for maximum salinity of 70,000 ppm.

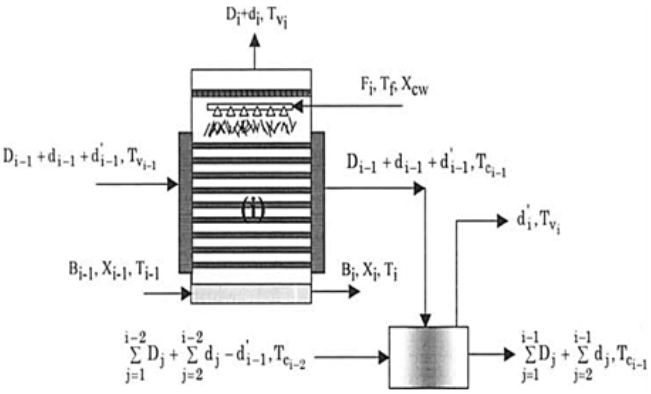

Fig. 2. Variables in the evaporator and the flash box in step i.

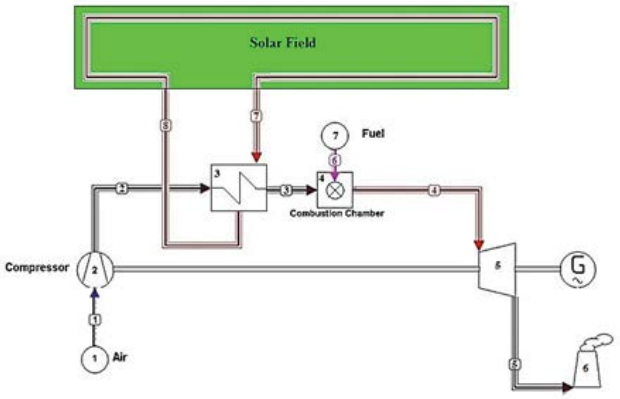

Fig. 3. View of gas turbine cycle with solar collector.

The energy balance for effect i is given by:

$$D_{i-1}\lambda_{i-1} + d_{i-1}\lambda_{i-1} + d'_{i-1}\lambda'_{i-1} = F_i C_p (T_i - T_f) + D_i\lambda_i \quad (19)$$

In Eq. (19) d is the vapor formed by the sudden evaporation of brine at effect i–1. λ is the latent heat, C_p is the specific heat at constant pressure, T_i is the boiling point of brine and T_f is the water supply temperature. The first part of Eq. (19) indicates the heat added to each effect with the steam condensation generated in the previous step. The second part of Eq. (19) is defined for steps 3 to n and refers to the amount of heat associated with the condensation formed by the sudden evaporation brine in the previous step. The third part, which applies only for effects 3 to n, refers to the heat added in each effect, due to the condensation of the steam generated in the flash box of the previous step. The fourth part of Eq. (19) is the amount of heat generated by the supply current, in which temperature rises from the water supply temperature to the boiling point. The final part is the amount of heat consumed by the steam generated in each step. In Eq. (19), the specific heat depends on the salinity of water and temperature, while the latent heat depends on the temperature of the steam. The steam temperature at effect i is as follows:

$$T_{vi} = T_i - \text{BPE}_i \quad (20)$$

BPE is the boiling point and T_v is the steam temperature. Also, the steam condensation temperature is as follows:

$$T_{ci} = T_i - \text{BPE}_i - \Delta T_p - \Delta T_t - \Delta T_c \quad (21)$$

In Eq. (21) the condensation temperature is lower than the boiling point T_i. Steam content due to sudden evaporation at each effect is as follows:

$$d_i = B_{i-1} C_p \frac{T_{i-1} - T'_i}{\lambda_i} \quad (22)$$

$$T'_i = T_i + \text{NEA}_i \quad (23)$$

In Eq. (23) T'_i is the temperature in which the brine cools down to enter the next step. The latent heat λ_i is also calculated at the steam temperature T_{vi} in the ith effect. The NEA_i section is computed from the following equation;

$$(\text{NEA}_i) = \frac{33\left(T_{i-1} - T_i\right)^{0.55}}{T_{v_i}} \quad (24)$$

$$d'_i = D_{i-1} C_p \frac{T_{c_{i-1}} - T''_i}{\lambda'_i} \quad (25)$$

$$T''_i = T_{vi} + \text{NEA}_i \quad (26)$$

$$(\text{NEA}_i) = \frac{0.33\left(T_{c_{i-1}} - T_{v_i}\right)}{T_{v_i}} \quad (27)$$

T''_i is the temperature when the condensed vapor is cooled down to enter the flash box.

The steam formation in steps 2 to n comprises two mechanisms, namely boiling and sudden evaporation

Steam flow formed in a flash box

$$D'_i = D_{i-1} C_p \frac{\left(T_{v_{i-1}} - T'_i\right)}{\lambda_i} \quad (28)$$

The cooling water flow comes from the following equation:

$$M_{cw} = \frac{D_N + D'_N - M_{ev}}{C_p\left(T_f - T_{cw}\right)} - M_f \quad (29)$$

$$(\text{LMTD})_i = (T_i - T_f)/\ln((T_{ci} - T_f)/(T_{ci} - T_i)) \quad (30)$$

LMTD is the logarithmic heat transfer coefficient and α is the fraction of the heat consumed during the formation of steam.

The equilibrium equations for a condenser include the energy balance and the heat transfer rate:

$$(d_n + d'_n + D_n)\,\lambda_n = U_c\, A_c\, (\text{LMTD})_C \quad (31)$$

$$(\text{LMTD})_C = (T_f - T_{cw})/\ln(T_{vn} - T_{cw})/(T_{cn} - T_f)) \quad (32)$$

A_c, U_c and $(\text{LMTD})_C$ respectively are the heat transfer surface, the total heat transfer coefficient, and the logarithmic average temperature difference.

In spite of the steam evaporator, the condensing heat load is less than the steam formed in the final effect and the vapor of the flash box, which enters the ejector. Thus, the steam formed in the last effect is defined as follows:

$$M_{ev} + M_u = (d_n + d'_n + D_n) \quad (33)$$

M_{ev} is the rate of steam flow to the evaporator and M_u steam is un-entrained (non-squeezing).

Calculation of salinity entropy in different locations of desalination is carried out using the following relation for pure water and salt.

$$s_i = s(P,T)_{i,\text{pure}} - R_u \ln_{xi} \quad (34)$$

The thermodynamic properties of the following relationships were obtained [22]:

$$H_f = -0.033635409 + 4.20755011T - 6.200339 \times 10^{-4} T^2 + 4.459374 \times 10^{-6} T^3 \quad (35)$$

$$H_g = 2501.689845 + 1.806916016T + 5.087717 \times 10^{-4} T - 1.221 \times 10^{-5} T^3 \quad (36)$$

$$\lambda = 2501.897149 - 2.407064037T + 1.192217 \times 10^{-3} T^2 - 1.5863 \times 10^{-5} T^3 \quad (37)$$

$$S_f = -0.00057846 + 0.015297489T - 2.63129 \times 10^{-5} T^2 + 4.11959 \times 10^{-8} T^3 \quad (38)$$

$$S_g = 9.149505306 - 2.581012 \times 10^{-2} T + 9.625687 \times 10^{-5} T^2 - 1.786615 \times 10^{-7} T^3 \quad (39)$$

$$T_{sat} = \left(42.6776 - \frac{3892.7}{\left[\ln\left(\frac{P}{1000} - 9.48654\right)\right]}\right) \quad (40)$$

4. Model of steam ejector

The steam ejector is taken from the El-Dessouky model [23]. C_r is the compression ratio defined as the compressive ratio to the vapor pressure of the input and E_r of the expansion ratio, as the ratio of the vapor pressure to the vapor pressure of the actuator. Ra the entrainment ratio is calculated as follows:

$$\text{Ra} = 0.296 \frac{\left(P_s\right)^{1.19}}{\left(P_{ev}\right)^{1.04}} \left(\frac{P_m}{P_{ev}}\right)^{0.015} \left(\frac{\text{PCF}}{\text{TCF}}\right) \quad (41)$$

P_m, P_s, and P_{ev} are respectively the pressure of the vapor of the actuator, the condensing steam, and the vapor suction. Pressure correction factor (PCF) is the stimulus steam pressure correction coefficient and temperature correction factor (TCF) is the refractive index of the steam evaporation temperature and are respectively calculated as follows:

$$\text{PCF} = 3 \times 10^{-7}(P_m)^2 - 0.0009(P_m) + 1.61 \tag{42}$$

$$\text{TCF} = 2 \times 10^{-8}(T_{ev})^2 - 0.0006(T_{ev}) + 1.0047 \tag{43}$$

The equations are valid for an entity that works under the following conditions:

$$\text{Ra} \le 4,\ 500 \ge T_{ev} > 10°\text{C},\ 3{,}500 \ge P_m \ge 100\ \text{kPa, and}\ 6 \ge C_r \ge 1.81 \tag{44}$$

The rate of vapor flow sucked from the last step and the input to the ejector (M_{ev}) is obtained from the following equations:

$$M_s = M_m \times \left(1 + \frac{1}{\text{RA}}\right) \tag{45}$$

$$M_{ev} = M_s - M_m \tag{46}$$

The performance factor of the sweetener is calculated from the following relationships:

$$D_{tot} = \sum_{i=1}^{N} D_i \tag{47}$$

$$\text{PR} = \frac{D_{tot}}{M_m} \tag{48}$$

One of the important characteristics of the heat-sweetening unit is heat consumption. This parameter refers to the thermal energy consumed by the system to produce 1 kg of freshwater and is calculated as follows:

$$Q = \frac{D_m \lambda_m}{D_t} \tag{49}$$

The flow of steam-driven is D_m, (kg/s), λ is the hidden heat (kJ/kg) and D_t is the total drinking water production that has been generated. The specific heat-transfer surface (A_d) is the sum of the heat transfer portions of the subunits and the condenser divided by the total product:

$$A_d = \frac{A_e + A_c}{D_t} \tag{50}$$

For power generation and desalination systems that are discussed here, the exergy efficiency is calculated from the following equation:

$$\eta_{ex} = \frac{E_p}{E_F} = \frac{W_{net} + E_d + E_b + E_{cw} - E_f}{E_{fuel}} \tag{51}$$

The network is W_{net}, the exergy of freshwater is E_d, the exergy of salty water is E_b, the exergy of cooling water is E_{cw} and exergy of water feed is E_f. The modeling of components of the combined cycle was performed, and the corresponding relationship codes are written with MATLAB software to reflect the outputs.

5. Gas turbine modeling

According to the formulas presented in the compressor model, combustion chamber and turbine, the thermodynamic characteristics of the various points of the cycle are presented in Table 1:

To find the exergy of different points of the cycle and calculate the exergy destruction, it is necessary to have enthalpy and entropy perspectives. According to the formulas presented in the combustion chamber modeling, the characteristics of different points of the cycle are stated in Table 2:

To find total exergy, it is needed to calculate the physical and chemical exergy in each of the points and the exergy destruction of each cyclic components is listed in Tables 3 and 4:

5.1. Sunshine duration and solar power reception in Iran

While 90% of regions in Iran have 300 sunny days a year, the average solar irradiance amounts to 5.5 kWh/m^2/d. The country's total solar power reception is then calculated as $5.5 \times 6.4 \times 12^{10}$ kWh/d. This means, if only 1% of the surface area that receives sunlight is covered with solar panels with 10% efficiency, then 9,000,000 MWh of solar energy could be utilized. Measurements of solar irradiance in Tehran indicate an average of 850–900 W/m^2 in summer and an average of 400–600 W/m^2 during winter.

5.2. Gas turbine with solar collector

If there are 1,000 collectors, before the combustion chamber, the thermodynamic characteristics of the various points of the cycle are presented in Table 5 and Specifications of different cycles in the application of 1,000 solar collectors are presented in Table 6.

Table 1
Thermodynamic characteristics of different points of the gas turbine cycle

Q (kJ/s)	T (K)	P (bar)	Point
240.00	300.00	1.013	1
240.00	628.50	10.13	2
244.39	1373.15	9.82	3
244.39	784.00	1.013	4
4.399	300.00	10.13	5

Table 2
Specifications without collector and flow of 240 kg/s

	T (K)	O_2	N_2	CO_2	H_2O	Mixture
$\bar{h}_1$ (kJ/kg)	300.15	60.00	20,200.00	–393,450.00	–241,790.00	10,810.80
$\bar{h}_2$ (kJ/kg)	628.50	10,230.00	29,990.00	–378,540.00	–230,030.00	20,858.90
$\bar{h}_3$ (kJ/kg)	1,373.15	35,810.00	54,320.00	–338,490.00	–198,970.00	19,134.40
$\bar{h}_4$ (kJ/kg)	784.00	15,330.00	34,920.00	–370,580.00	–223,970.00	–1,948.65
$\bar{S}_1^0$ (kJ/K)	300.15	205.33	191.80	214.03	189.04	–
$\bar{S}_2^0$ (kJ/K)	628.50	228.08	214.11	246.98	215.22	–
$\bar{S}_3^0$ (kJ/K)	1,373.15	254.73	239.52	288.70	247.49	–
$\bar{S}_4^0$ (kJ/K)	784.00	235.32	221.11	258.28	223.83	–
$\bar{S}_1$ (kJ/K)	300.15	218.19	193.88	280.02	221.28	199.43
$\bar{S}_2$ (kJ/K)	628.50	222.21	197.46	294.24	228.74	203.18
$\bar{S}_3$ (kJ/K)	1,373.15	252.22	223.12	297.96	249.11	239.18
$\bar{S}_4$ (kJ/K)	784.00	251.29	223.19	286.02	243.94	238.27

Table 3
Exergy without the collector and flow of 240 kg/s

Exergy [kJ/s]			Point
Total exergy	Physical exergy	Chemical exergy	
129,577	129,577	0	1
204,399	204,399	0	2
167,635	101,833	65,802	3
9,857	75,659	65,802	4
246,549	24,649	221,900	5

Table 4
Exergy destruction without collector and flow of 240 kg/s

Exergy destruction [kJ/s]	
2,365,500	Compressor
0	Exchanger
349,111	Combustion
4,882,400	Turbine

With the use of 1,000 collectors and 240 kg/s flow, the physical and chemical exergy of each of the combined cycle points is as Table 7 and the exergy destruction of each component of the combined cycle is listed in Table 8:

6. Results and discussion

Fig. 4 shows the mass-flow changes in CO_2 production and fuel consumption with the number of collectors, as the number of solar collector's increases, the amount of fuel mass and the mass flow of CO_2 produced are reduced. With the use of 2,000 collectors, the amount of fuel consumed from 4.4 kg/s is reduced to less than 2 kg/s, and the amount of CO_2 produced from 12 kg/s is reduced to 6.2 kg/s. With the use of 1,000 solar collectors, the amount of fuel is reduced to 3.322 kg/s and CO_2 emissions to 9.2 kg/s.

Table 5
Thermodynamic characteristics of different points of the gas turbine cycle using a solar collector (1,000 collectors)

$\dot{m}$(kg/s)	T (K)	P (bar)	Point
240.00	300.00	1.013	1
240.00	628.50	10.13	2
240.00	800.50	10.13	3
243.32	1373.15	9.82	4
243.32	784.00	1.013	5
3.322	300.00	10.03	6
354.36	1,100.00	–	7
354.36	1,000.00	–	8

As shown in Fig. 5, increasing the airflow the fuel consumption also increases, but with the increasing number of collectors, the fuel consumption is reduced. In non-collector mode and 240 kg/s airflow, the fuel consumption is 4.4 kg/s, which is reduced by the use of 2,000 collectors up to 2.5 kg/s, which amounts to a significant amount annually. Also, with the use of 1,000 solar collectors, fuel consumption is reduced to 3.322 kg/s.

According to Fig. 6, CO_2 production decreases by increasing the number of solar collectors. In the case of not utilizing collectors, with an airflow rate of 240 kg/s, the CO_2 production rate is 12 kg/s which decreases by half when using 2,000 solar collectors and has a significant annual value. If using 1,000 solar collectors, CO_2 production decreases to 9.2 kg/s.

Table 6
Specifications with the number of 1,000 collectors and flow of 240 kg/s

	T (K)	O_2	N_2	CO_2	H_2O	Mixture
$\bar{h}_1$ (kJ/kg)	300.15	60.00	20,200.00	–393,450.00	–241,790.00	10,810.80
$\bar{h}_2$ (kJ/kg)	628.50	10,230.00	29,990.00	–378,540.00	–230,030.00	20,858.90
$\bar{h}_3$ (kJ/kg)	800.50	15,890.00	35,460.00	–369,710.00	–223,300.00	26,389.20
$\bar{h}_4$ (kJ/kg)	1,373.15	35,810.00	54,320.00	–338,490.00	–198,970.00	25,322.20
$\bar{h}_5$ (kJ/kg)	784.00	15,330.00	34,920.00	–370,580.00	–223,970.00	4,554.28
$\bar{S}_1^0$ (kJ/K)	300.15	205.33	191.80	214.03	189.04	–
$\bar{S}_2^0$ (kJ/K)	628.50	228.08	214.11	246.98	215.22	–
$\bar{S}_3^0$ (kJ/K)	800.50	236.03	221.79	259.39	224.68	–
$\bar{S}_4^0$ (kJ/K)	1,373.15	254.73	239.52	288.70	247.49	–
$\bar{S}_5^0$ (kJ/K)	784.00	235.32	221.11	258.28	223.83.00	–
$\bar{S}_1$ (kJ/K)	300.15	218.19	193.88	280.02	221.28	199.43
$\bar{S}_2$ (kJ/K)	628.50	222.21	197.46	294.24	228.74	203.18
$\bar{S}_1$ (kJ/K)	800.50	230.16	205.14	206.64	238.19	210.95
$\bar{S}_4$ (kJ/K)	1,373.15	251.38	223.12	300.11	250.74	236.98
$\bar{S}_5$ (kJ/K)	784.00	250.45	223.19	288.17	245.57	236.22

Table 7
Exergy with the number of 1,000 collector and 240 kg/s flow

Exergy (kJ/s)			Point
Total exergy	Physical exergy	Chemical exergy	
129,577	129,577	0	1
204,399	204,399	0	2
231,311	231,311	0	3
200,978	159,533	41,445	4
26,469	14,948	41,445	5
189,661	18,961.25	170,700	6
508.49	508.49	0	7
464.31	464.31	0	8

Table 8
Exergy destruction with the number of 1,000 collector and 240 kg/s flow

Exergy destruction (kJ/s)	
2,365,500	Compressor
26,877	Exchanger
261,433	Combustion
4,809,800	Turbine

Fig. 7 shows that for airflow of 240 kg/s and 2,000 collectors, the temperature difference is 350 degrees and with 1,000 collectors this value decreases to 180 degrees. This means that the air is pre-heated with the application of collectors before entering the combustion chamber.

Fig. 8 illustrates that with airflow of 240 kg/s and 1,000 collectors, the temperature increases up to 680°C with 2,000 collectors.

The efficiency of the system is plotted against airflow and many collectors in Fig. 9. With an airflow of 240 kg/s and no collectors, the efficiency is 37% which increases to 45% and 60% for 1,000 and 2,000 collectors, respectively.

Fig. 10 shows that salt consumption increases with the number of collectors. For approximately 1,000 collectors, the salt consumption is 350 kg/s which means 3.5 kg/s/collector if we assume 10 rows of 100 collectors.

The collection is different in Fig. 11 and is based on the combustion chamber inlet temperature and airflow mass rate for a different number of collectors. With 1,000 collectors and 240 kg/s airflow, it is seen that the combustion chamber inlet temperature is 800.5 K. Also, different inlet temperatures for different number of collectors and airflow values can be extracted from that chart

In Fig. 12, exchanger area and many collectors are plotted against different airflow rates which can be used with the exchanger model mentioned in the reference to extract the required number of exchanges in each cycle.

Fig. 13 shows that by increasing the combustion chamber temperature from 628.5 to 828.5 K, energy and exergy efficiencies increase from 37% and 38% to 45% and 48%, respectively.

It can be seen in Fig. 14 that increasing the number of collectors causes a decrease in exergy destruction and the exergy destruction rate is higher in lower airflow rates.

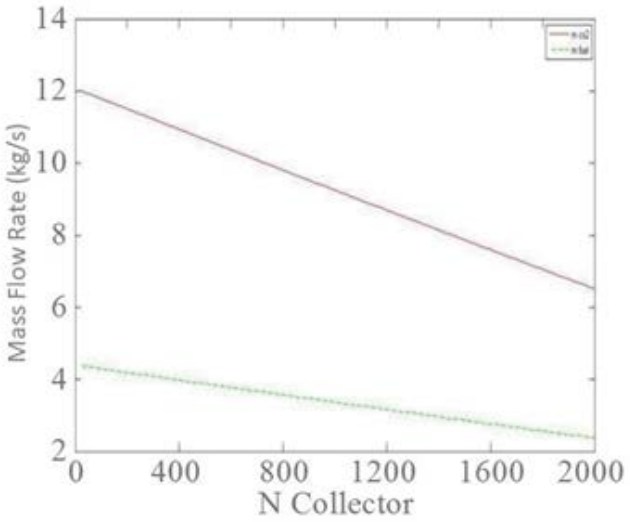

Fig. 4. Mass-flow changes in CO_2 production and fuel consumption with the number of collectors.

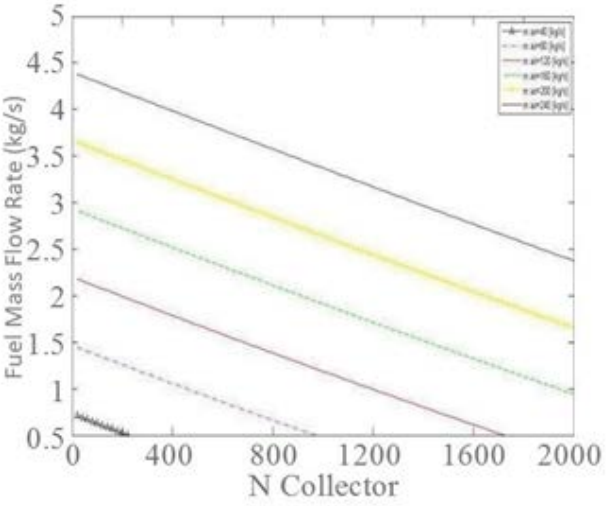

Fig. 5. Fuel consumption rate in different air flows in terms of collector numbers.

Fig. 15 shows that the exergy destruction rate is lower in the case of 1,000 collectors compared to the case of no collectors and that the exergy destruction rate increases with increasing airflow. The amount of decrease of exergy destruction is higher in low airflow.

According to the equation presented in the modeling of the desalination system section, the distillate production of each effect and other parameters can be calculated as shown in Table 9. System operation parameters are presented in Table 10.

Exergy destruction of each effect is presented in Table 11 and ejector design parameters are shown in Table 12. Fig. 16 shows the effect of temperature on the saltiness of the outlet water and it can be seen from the figure that inlet temperature increase in the first operator causes the decrease of the salt in the final operator outlet.

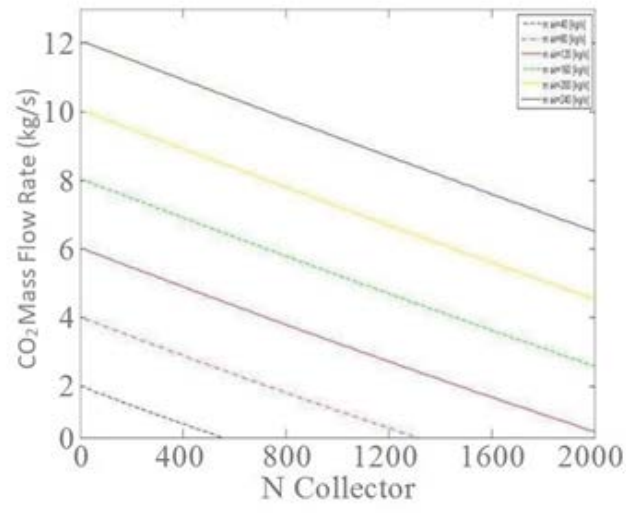

Fig. 6. CO_2 production rate of different air flow rate for the number of collectors.

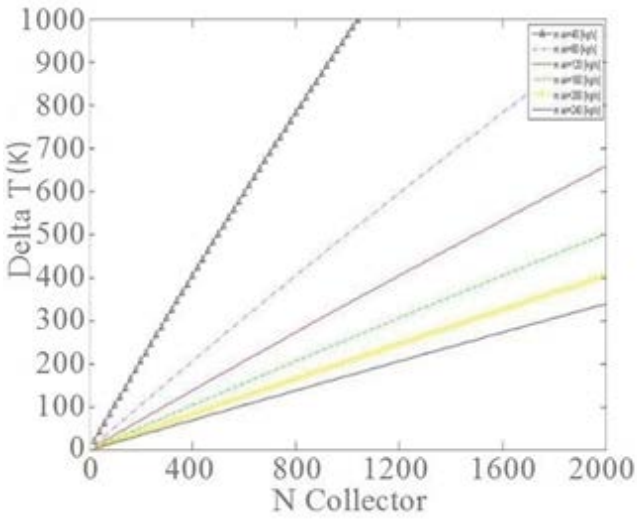

Fig. 7. Temperature changes due to solar panels with respect to different air flow and number of collectors.

Fig. 17 also shows higher rates of salt increased in the first three operators due to their higher temperatures compared to the rest of the operators. According to Fig. 17, increasing the temperature of the first operator inlet causes a decrease in distillate produce amount.

Due to the definition of gained output ratio and the assumption that the motive steam flow rate is constant and distillate produce decreases with T_1 increase, the diagram should have a linearly decreasing trend which is demonstrated in Fig. 18, as expected.

Calculating the ratio of motive steam to entrained steam in the ejector is an important part of MED-TVC modeling. The optimum value of this parameter increases the system efficiency by reducing the amount of motive steam. The expansion ratio is the ratio between the motive steam

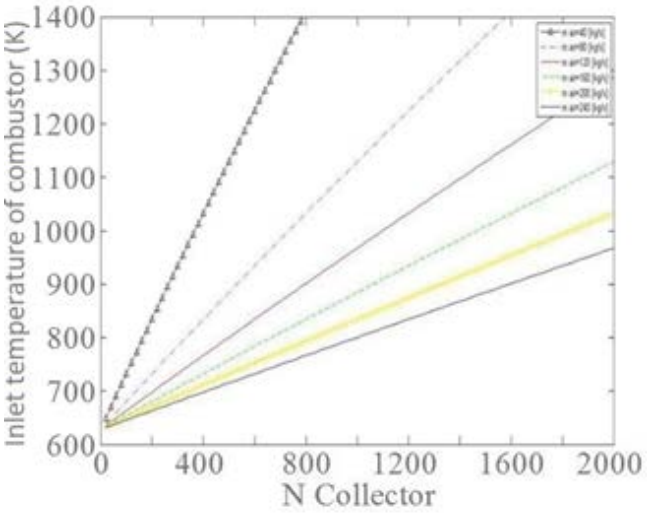

Fig. 8. Combustion chamber inlet temperature increase.

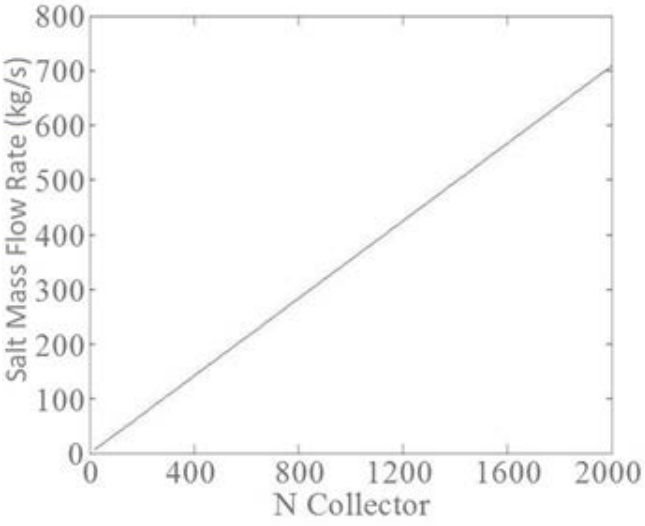

Fig. 10. Variation of sodium liquid mass flow rate with different number of collectors.

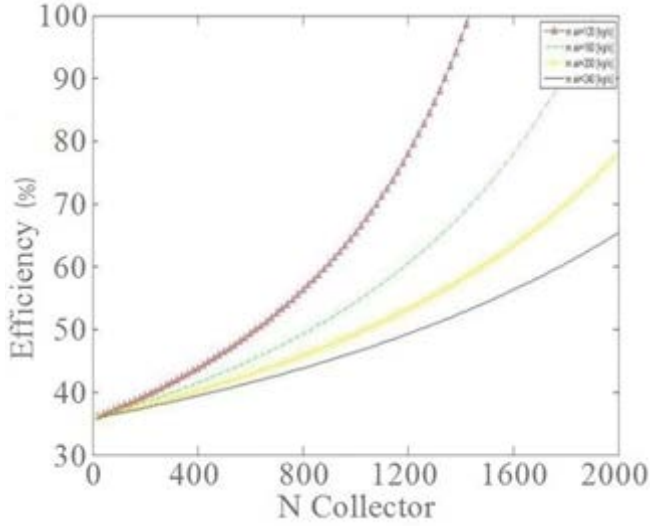

Fig. 9. Efficiency versus different air flow values and number of collectors.

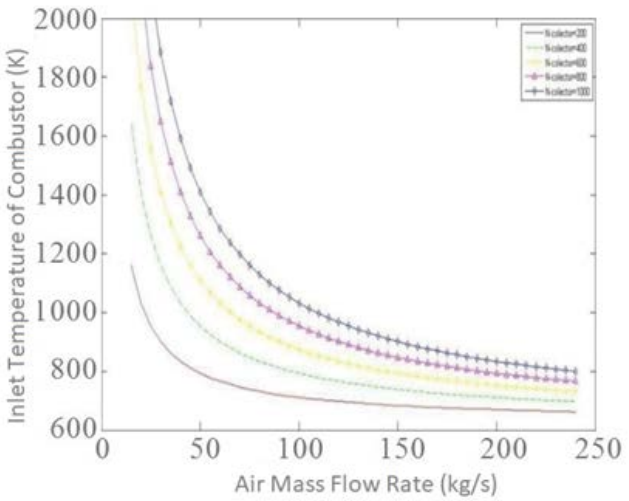

Fig. 11. Combustion chamber inlet temperature versus air flow mass rate in different number of collectors.

pressure and entrained pressure which, according to Fig. 19, decreases with an increase in T_1. Calculating the ratio of motive steam to entrained steam in the ejector is an important part of MED-TVC modeling. The optimum value of this parameter increases the system efficiency by reducing the amount of motive steam.

The entrainment ratio is a function of compression pressure, motive pressure, and entrained pressure. As shown in Fig. 20, increasing T_1 causes an increase in entrainment ratio. The specific heat transfer area is the sum of all effects and condenser's heat transfer areas divided by total distillate produce.

It can be seen in Fig. 21 that the temperature T_1 increase (as in Fig. 17) causes distillate production to decrease, thus decreasing the specific heat transfer area. One of the most important parameters of the heat desalination systems is the specific heat consumption. This parameter refers to the heat energy required to produce 1 kg of distillate water.

According to the previous discussions, with constant motive pressure and decreasing distillate produce, specific heat consumption increases. As shown in Fig. 22, temperature T_1 increases specific heat consumption.

Fig. 23 illustrates that temperature T_1 increase causes exergy to decrease. It can be seen form Fig. 24 that temperature T_1 increase causes exergy destruction to increase.

Fig. 25 shows that the energy efficiency of simultaneous power production and desalination system increases by increasing the combustion chamber temperature. Using 1,000 collectors, energy efficiency increases from 47.13% to 60.59%, and by using 2,000 collectors, it increases to 84.74%. According to Fig. 26, the exergy efficiency of simultaneous power production

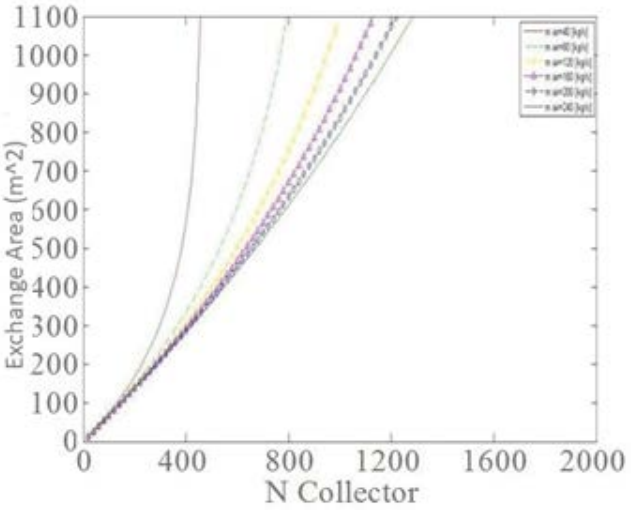

Fig. 12. Variation of exchanger area and number of collectors for different air flow rates.

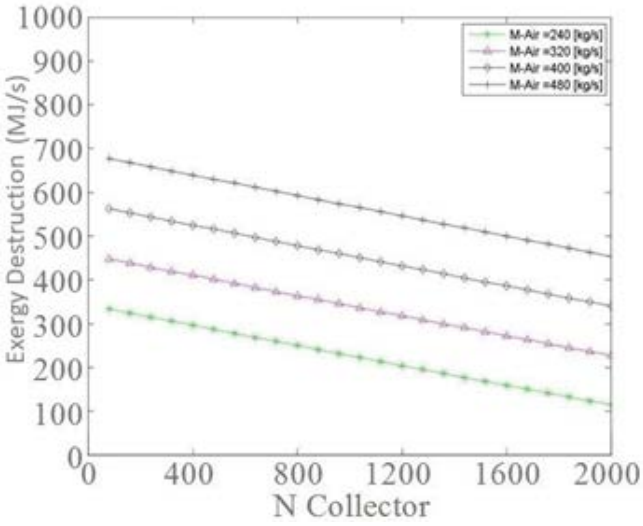

Fig. 14. exergy destruction of different air flows for different number of collectors.

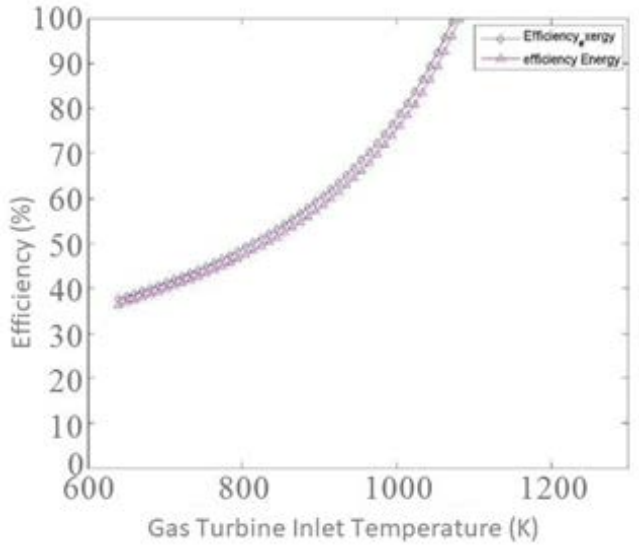

Fig. 13. energy and exergy efficiencies for various GTIT.

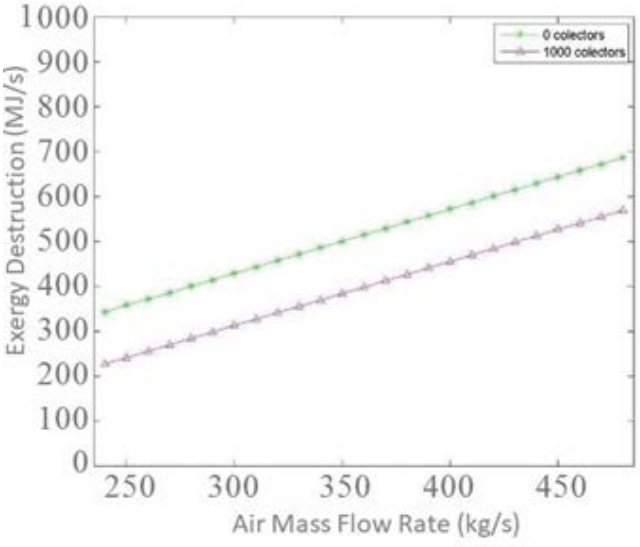

Fig. 15. exergy destruction of different number of collectors for different air flow values.

Table 9
Properties of each effect of the desalination system

Effect	1	2	3	4	5	6
D (kg/s)	33.720	32.202	31.280	30.877	30.993	31.660
B (kg/s)	22.643	46.809	71.896	97.387	122.761	147.469
X (ppm)	45,664.560	46,575.600	58,548.220	64,060.070	67,348.640	69,825.100
T (°C)	71.000	66.7100	61.796	56.7100	51.394	45.7810
A (m²)	6,964.960	8,218.887	7,175.552	7,177.503	7,187.803	7,210.842

Table 10
System operation parameters

D (kg/s)	190.736	Amount of fresh water produced
PR	8.151	Sweetening performance factor
Q (kJ/kg)	226.394	Specific heat consumption
A_d (m^2/(kg/s))	238.853	Special heat transfer surface

Table 11
Exergy destruction (kJ/s) of each effect

ED_c	7,202,186.647	Condenser
ED_{ev}	16.789	Suction steam
ED_f	4,672.776	Water supply
ED_b	46.916	Salty water
	40.317	Total destruction exergy of special evaporators (kJ/kg)

Table 12
Ejector design parameters

CR	4.388	Compression ratio
ER	267.320	Expansion ratio
Ra	2.077	Suction ratio

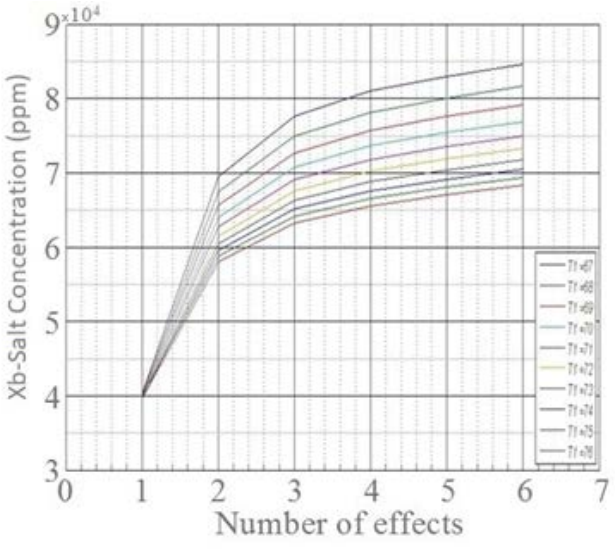

Fig. 16. Effect of temperature variation on saltiness of the outlet water.

and desalination system increases by increasing the combustion chamber temperature.

Using 1,000 collectors, energy efficiency increases from 39.43% to 50.55%, and by using 2,000 collectors, it increases to 70.52%.

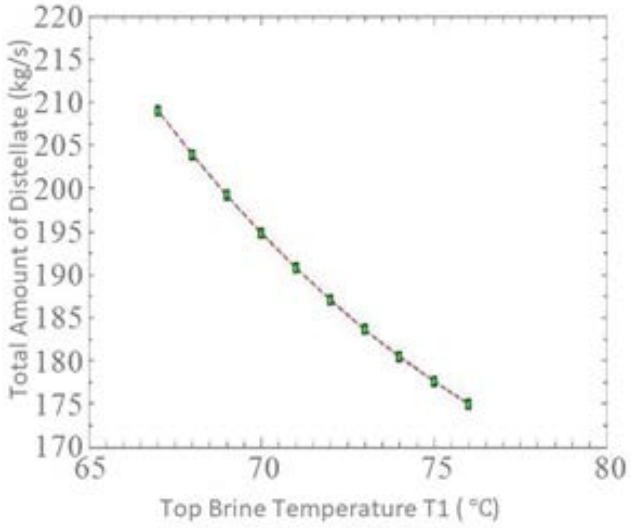

Fig. 17. Effect of temperature variation on distillate produce.

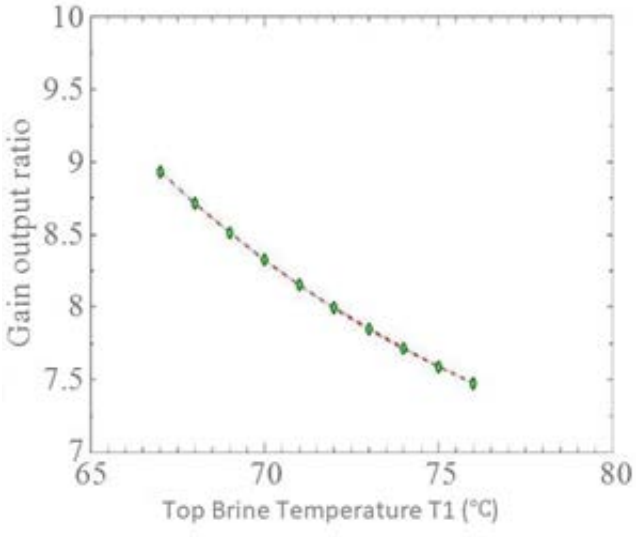

Fig. 18. Effect of temperature variation on gain output ratio.

7. Conclusion

In this study, the use of solar power to heat the inlet air of the combustion chamber of a gas turbine was assessed. This method decreased fuel consumption which resulted in increased cycle efficiency. Assuming 300 sunny days and using 1,000 solar collectors for 9 h/d to increase the inlet air temperature from 628.5 to 800.5 K, the system energy and exergy efficiencies increased significantly. Initial energy and exergy efficiencies values were 35% and 37%, respectively, which increased to the significant values of 46% and 48% after increasing the inlet air temperature. As shown in the graphs, increasing the number of collectors can increase the efficiency up to 60%. Furthermore, in the combined system of gas turbines and parabolic solar collectors, exergy destruction decreased, which showed more noticeable decrease in lower air flows. It is also worth noting

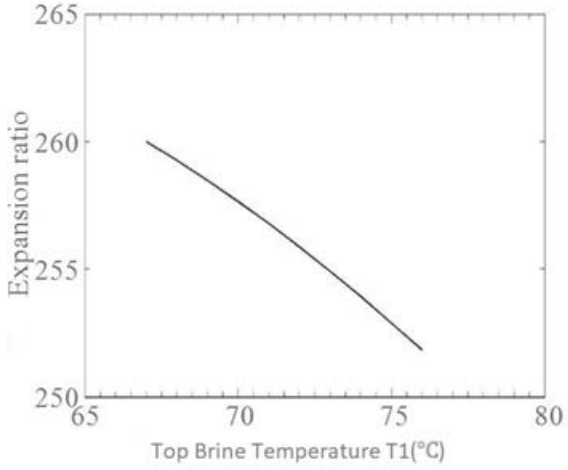

Fig. 19. Effect of temperature variation on expansion ratio.

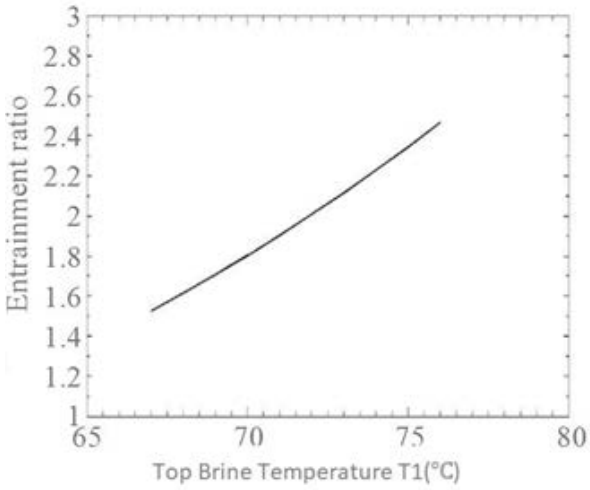

Fig. 20. Effect of temperature variation on entrainment ratio.

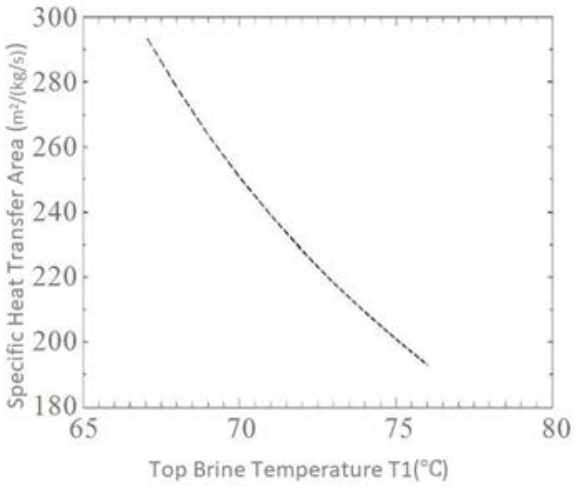

Fig. 21. Effect of temperature variation on specific heat transfer area.

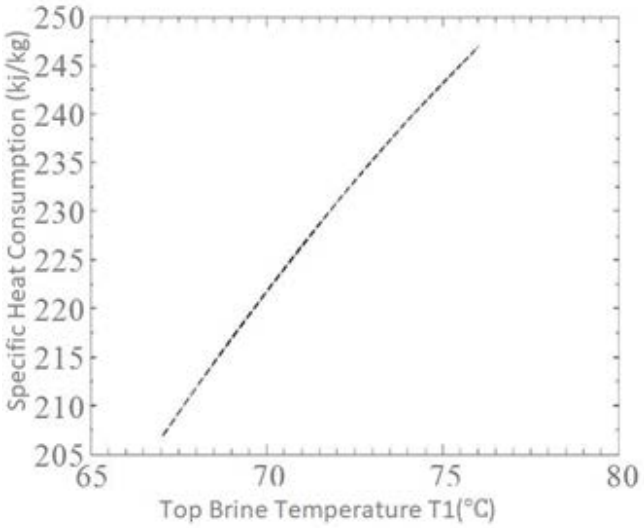

Fig. 22. Effect of temperature variation on specific heat consumption.

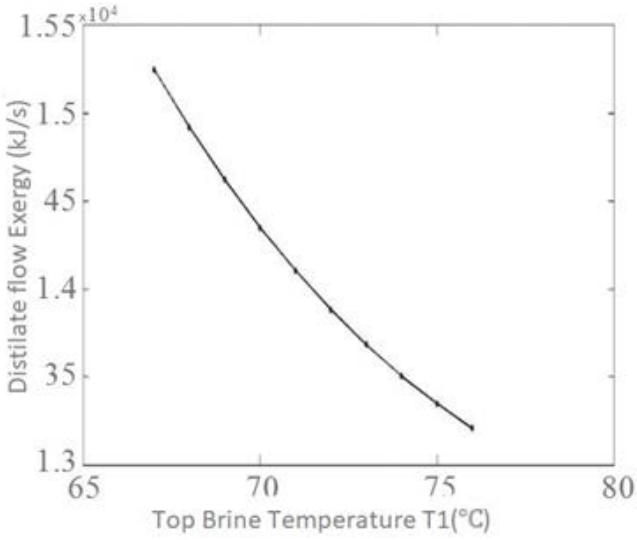

Fig. 23. Effect of temperature variation on exergy.

that the above method decreased the fuel consumption by 15.95 MCM per annum and decreased the Carbon Dioxide emission by 37,216 tons. Assuming the gas price of 0.0714 $/$m^3$ the fuel consumption decreases by 1.14 million US dollars and CO_2 price of 23.8 $/ton resulting in saving of 0.6478 million dollars, with the total value of saving 1.7876 million dollars per year. On the other hand, reaching the aforementioned solar power production requires significant investment which can be considered by taking into account the environmental values of the proposed method. Moreover, the hot outlet gas of the turbine was used to produce steam needed for the desalination system. In the proposed system a recycling boiler was used to increase the efficiency of the heat cycle. Reusing the excess heat in the system reduced the fuel consumption and the final price. In the simultaneous power production and desalination system, the

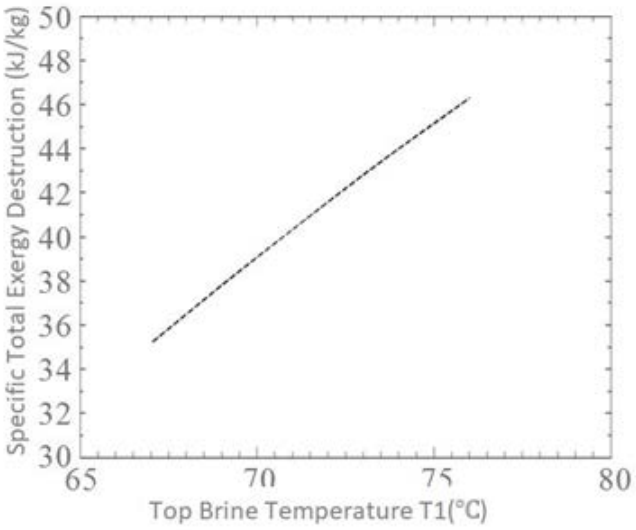

Fig. 24. Illustrates that temperature T_1 increase causes exergy to decrease.

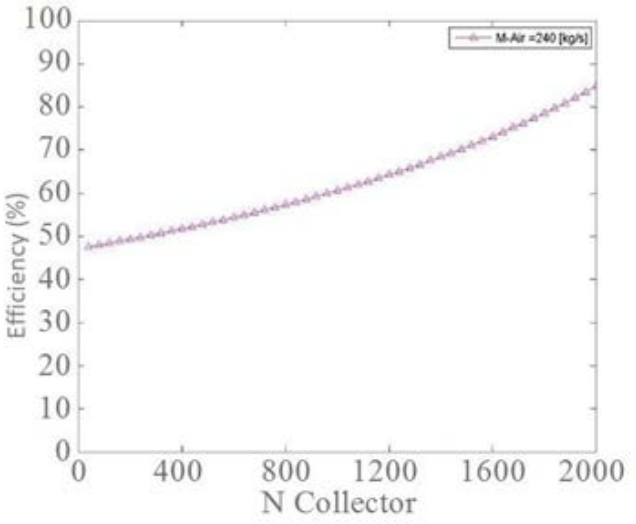

Fig. 25. Effect of temperature variation on exergy destruction.

amount of distillate produce was estimated 16.479 m^3/d. By increasing the combustion chamber temperature using the collectors, exergy efficiency was increased. By using 1,000 collectors, exergy efficiency was increased from 39.43% to 50.55% and by using 2,000 collectors, the exergy efficiency increased to 70.52%.

Symbols

A	—	Area, m^2
C	—	Concentration ratio
C_p	—	Specific heat capacity under constant pressure, J/kg K
D	—	Diameter, mm
E	—	Exergy flow, W
F	—	Focal length, mm

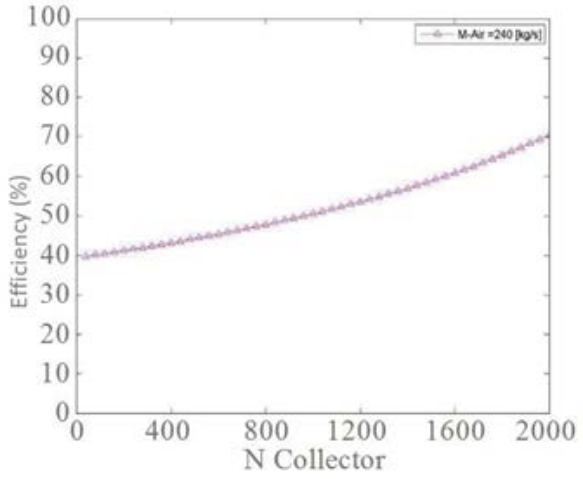

Fig. 26. Exergy efficiency of simultaneous power production and desalination system.

Gb	—	Solar beam radiation, W/m^2
h	—	Convection coefficient, W/m^2 K
h_{out}	—	Convection coefficient between cover and ambient, W/m^2 K
L	—	Tube length, mm
M	—	Mass flow rate, kg/s
Q	—	Heat flux, W
T	—	Temperature, K
W	—	Width, mm

Greek symbols

ε	—	Emittance
η	—	Efficiency
ΔT_m	—	Log mean temperature difference

Subscripts and superscripts

a	—	Aperture
am	—	Ambient
c	—	Cover
ci	—	Inner cover
co	—	Outer cover
ex	—	Exergetic
in	—	Inlet
opt	—	Optical
out	—	Outlet
r	—	Receiver
ri	—	Inner receiver
ro	—	Outer receiver
s	—	Solar
sun	—	Sun
th	—	Thermal
u	—	Useful

Abbreviations

CCPP	—	Combined Cycle Power Plant
CHP	—	Combined Heat and Power
HRSG	—	Heat Recovery Steam Generator

HTF	—	Heat Transfer Fluid
LHV	—	Lower Heating Value, kJ/kg
PTC	—	Parabolic trough collector

References

[1] E. Bellos, C. Tzivanidis, K.A. Antonopoulos, A detailed working fluid investigation for solar parabolic trough collectors, Appl. Therm. Eng., 114 (2017) 374–386.

[2] S. Sanaye, V. Mahdikhani, Z.K. Karimeddini, G. Sadri, Thermal and Economic Analysis of Gas Turbine Steam Injection Plant, Vol. 4, Cycle Innovations; Electric Power; Industrial and Cogeneration; Manufacturing Materials and Metallurgy, ASME, 2006, p. 785.

[3] N. Kahraman, Y.A. Cengel, Exergy analysis of a MSF distillation plant, Energy Convers. Manage., 46 (2005) 2625–2636.

[4] S.E. Shakib, S.R. Hosseini, M. Amidpour, C. Aghanajafi, Multi-objective optimization of a cogeneration plant for supplying given amount of power and fresh water, Desalination, 286 (2012) 225–234.

[5] K. Maghsoudi, M. Aliasghari, A. Mehrpanahi, Thermoeconomic investigation of coupling MED-TVC with a combined cycle power plant, Desal. Wat. Treat., 57 (2016) 17707–17721.

[6] A. Bejan, G. Tsatsaronis, M.J. Moran, M. Moran,Thermal Design and Optimization, ISBN: 978-0-471-58467-4, Wiley, 1996. Available at: https://www.wiley.com/en-us/Thermal+Design+and+Optimization-p 9780471584674 (accessed June 29, 2019).

[7] J.K. Fink, L. Leibowitz, Calculation of Thermophysical Properties of Sodium, (CONF-8106164--5), United States, 1981. Available at: https://inis.iaea.org/search/search.aspx?orig_q=RN:14776927 (accessed June 29, 2019).

[8] V. Ariu, A. Pautz, H.-M. Prasser, K. Mikityuk, C. Fiorina, Heat Exchanger Analysis for Innovative Molten Salt Fast Reactor, 2014. Available at: https://www.psi.ch/sites/default/files/import/fast/PublicationsEN/FB-DOC-14-020.pdf (accessed June 29, 2019).

[9] A. Sharif, Modelling of a Natural-Gas-Based Clean Energy Hub, 2012. Available at: https://uwspace.uwaterloo.ca/handle/10012/6674?show=full (accessed June 29, 2019).

[10] I.S. Al-Mutaz, I. Wazeer, Development of a steady-state mathematical model for MEE-TVC desalination plants, Desalination, 351 (2014) 9–18.

[11] P. Ahmadi, M.A. Rosen, I. Dincer, Multi-objective exergy-based optimization of a polygeneration energy system using an evolutionary algorithm, Energy, 46 (2012) 21–31.

[12] S. Hoseinzadeh, R. Azadi, Simulation and optimization of a solar-assisted heating and cooling system for a house in Northern of Iran, J. Renewable Sustainable Energy, 9 (2017) 045101.

[13] M.A. Javadi, S. Hoseinzadeh, M. Khalaji, R. Ghasemiasl, Optimization and analysis of exergy, economic, and environmental of a combined cycle power plant, Sādhanā - Acad. Proc. Eng. Sci., 44 (2019) 121.

[14] S. Hoseinzadeh, M. Hadi Zakeri, A. Shirkhani, A.J. Chamkha, Analysis of energy consumption improvements of a zero-energy building in a humid mountainous area, J. Renewable Sustainable Energy, 11 (2019) 015103.

[15] M.A. Javadi, S. Hoseinzadeh, R. Ghasemiasl, P.S. Heyns, A.J. Chamkha, Sensitivity analysis of combined cycle parameters on exergy, economic, and environmental of a power plant, J. Therm. Anal. Calorim., (2019) 1–7, doi: 10.1007/s10973-019-08399-y.

[16] P. Ahmadi, I. Dincer, M.A. Rosen, Exergy, exergoeconomic and environmental analyses and evolutionary algorithm based multi-objective optimization of combined cycle power plants, Energy, 36 (2011) 5886–5898.

[17] M.A. Javadi, H. Ghomashi, Thermodynamics analysis and optimization of abadan combined cycle power plant, Indian J. Sci. Technol., 9 (2016), doi: 10.17485/ijst/2016/v9i7/87770.

[18] M.E. Yousef Nezhad, S. Hoseinzadeh, Mathematical modelling and simulation of a solar water heater for an aviculture unit using MATLAB/SIMULINK, J. Renewable Sustainable Energy, 9 (2017) 063702.

[19] S. Hoseinzadeh, P.S. Heyns, A.J. Chamkha, A. Shirkhani, Thermal analysis of porous fins enclosure with the comparison of analytical and numerical methods, J. Therm. Anal. Calorim., 138 (2019) 727–735.

[20] S. Hoseinzadeh, A. Moafi, A. Shirkhani, A.J. Chamkha, Numerical validation heat transfer of rectangular cross-section porous fins, J. Thermophys. Heat Transfer, 33 (2019) 1–7.

[21] K.A. Khalid, M.A. Antar, A. Khalifa, O.A. Hamed, Allocation of thermal vapor compressor in multi effect desalination systems with different feed configurations, Desalination, 426 (2018) 164–173.

[22] E. Hu, Y.P. Yang, A. Nishimura, F. Yilmaz, A. Kouzani, Solar thermal aided power generation, Appl. Energy, 87 (2010) 2881–2885.

[23] H.T. El-Dessouky, H.M. Ettouney, Fundamentals of Salt Water Desalination, ISBN: 9780444508102, Elsevier, 2002.